WILEY Journal of Applied Polymer Science

On The Use Of Ball Milling To Develop PHBV-Graphene Nanocomposites (II) – Mechanical, Barrier And Electrical Properties

Journal:	*Journal of Applied Polymer Science*
Manuscript ID:	APP-2014-12-4264
Wiley - Manuscript type:	Research Article
Keywords:	composites, biomaterials, Biopolymers & renewable polymers, nanotubes, graphene and fullerenes, biodegradable

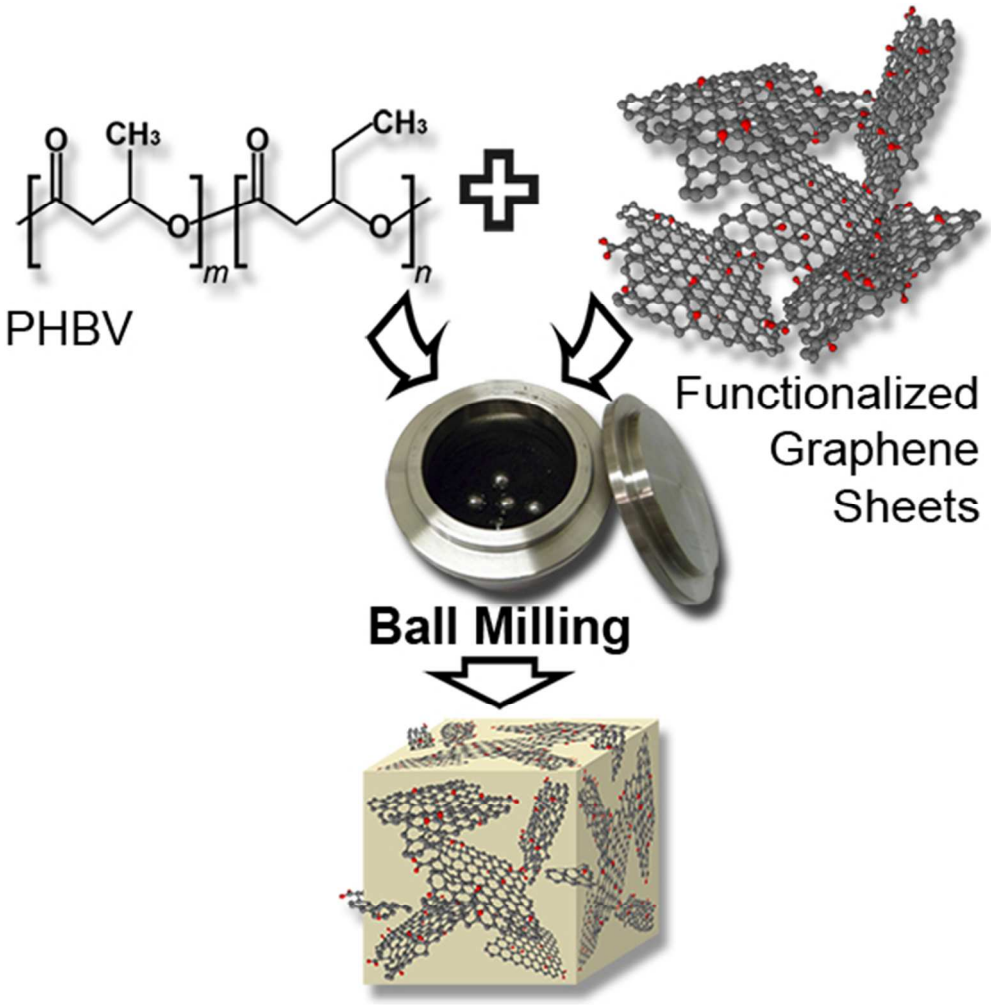

50x50mm (300 x 300 DPI)

On The Use Of Ball Milling To Develop PHBV-Graphene Nanocomposites (II) – Mechanical, Barrier And Electrical Properties

Jesús Ambrosio-Martín[a], Giuliana Gorrasi[b]*, Amparo Lopez-Rubio[a], María José Fabra[a], Luís Cabedo Mas[c], Miguel Angel López-Manchado[d], and Jose María Lagaron[a]*

[a]Novel Materials and Nanotechnology Group, IATA, CSIC, Av. Agustín Escardino 7, 46980 Paterna (Valencia), Spain.

[b]Department of Industrial Engineering University of Salerno, Via Giovanni Paolo II 132, 84084 Fisciano Salerno Italy

[c]ESID, Universitat Jaume I, Avda. Vicent Sos Baynat s/n, 12071 Castellón, Spain

[d]Institute of Polymer Science and Technology, (CSIC), Juan de la Cierva, 3, 28006 Madrid, Spain

*Authors to whom correspondence can be addressed.

Tel: +34 963900022

Tel: +39 089964146

Abstract

In this study, poly (3-hydroxybutyrate-co-3-hydroxyvalerate) (PHBV) nanocomposites containing functionalized graphene sheets (FGS) were prepared by means of high energy ball milling. The crystalline structure, oxygen barrier, mechanical and electrical properties of the developed nanocomposites were analysed and correlated with the amount of FGS incorporated. Moreover, the biodisintegration in composting conditions of the different samples was also studied. Addition of FGS into the PHBV matrix did not affect the crystalline form of the material. The good dispersion of the nanofillers within the polymeric matrix, which led to a good filler-matrix adhesion, as revealed in the first part of this study, was crucial for the reinforcing effect of FGS and also resulted in enhanced barrier properties to oxygen at high relative humidity. Finally, the conducting behaviour of the nanocomposites, interpreted by the percolation theory, displayed a very low percolation threshold of ~0.3 vol% of FGS. Addition of FGS also resulted in accelerated biodisintegration, although in less than 75 days, all the samples studied, even neat PHBV, reached 90% biodisintegration.

Keywords: barrier properties, graphene, nanocomposites, ball milling, polyhydroxyalkanoates

1. Introduction

Graphene, a two dimensional material consisting of a single layer of carbon atoms packed in a hexagonal lattice, has gained much attention in last years due to its remarkable physical properties. Specifically, due to their outstanding mechanical, thermal and electrical properties, graphene materials are expected to be used in a variety of applications, including sensors, batteries, supercapacitors, hydrogen storage systems and as reinforcement fillers in nanocomposites[1].

Besides the reinforcing effect of this nanofiller, graphene has a lamellar structure which can, thus, act as a barrier element in polymer nanocomposites decreasing gas permeability[2]. Several studies in the literature have corroborated this high barrier effect of graphene-based nanofillers in polymer matrices[3-5].

Among all the processes for the production of graphene, e.g. mechanical exfoliation, chemical exfoliation, chemical vapour deposition or epitaxial growth, the reduction of graphene derivatives such as graphene oxide has attracted more attention since it is a strategy able to produce graphene sheets in both colloidal dispersions and powder forms with high processability. Moreover, the presence of oxygen functionalities in the graphene oxide is very interesting from a chemical point of view. Therefore, this material is expected to serve as nanofiller in nanocomposite applications since they provide reactive sites for chemical interaction which will favor interaction with the matrix[1, 6].

The most well-known processes to prepare polymer nanocomposites are solution casting, in-situ polymerization and melt compounding[7]. Graphene-based nanocomposites with improved mechanical, thermal, electrical and/or barrier properties have been already developed using the above-mentioned methods[2, 4, 8-12]. A novel strategy that is being explored for the development of nanocomposites is the ball milling

technique, which has demonstrated to be especially interesting for clay-based and carbon-based nanocomposites[13, 15-18]. This technique is based in a high-energy milling, able to induce several mechanical and chemical changes in the materials.

Regarding the polymer matrices to be used for graphene-based nanocomposites development, matrices such as PVA[19], polyethylene (PE)[20] and polystyrene (PS)[21], among others, have already been used. In the last years great interest has been focused on biopolymers due to the emerged environmental concerns about the use of petroleum-based polymers regarding its fossil-resources dependence and also its low degradation rate. Polyhydroxyalcanoates have gained much attention not only due to their environmentally-friendly properties such as biodegradability, biocompatibility and renewable features but also these materials have mechanical properties similar to those of conventional petroleum-based polymers, relatively good thermal properties and high stiffness due to its high crystallinity degree[22].

However, these biopolymers have some drawbacks, such as high brittleness, processing difficulty and low thermal stability, which should be improved to extend their field of applications[2, 22].

In the first part of this study, functionalized graphene sheets were introduced into PHBV by means of high energy ball milling (HEBM). The morphology, thermal properties and thermal stability of the obtained materials were evaluated and it was found that this technique led to a relatively good dispersion and distribution of the nanofiller within the polymer matrix, which inferred improved crystallinity due to the nucleating effect of the FGS. In the present work, the crystalline structure, mechanical, barrier and electrical properties of the nanocomposites developed are evaluated, and related to the analysed morphological and thermal characterization.

2. Experimental Section

2.1 Materials

The bacterial polyhydroxyalkanoate grade was purchased from Goodfellow Cambridge Limited, UK, in pellet form (density 1.25 g cm^{-3}). The supplied material was a melt-processable semicrystalline thermoplastic PHBV12 (polyhydroxybutyrate with 12 mol% of valerate and containing 10 wt% of the plasticizer citric ester) copolymer made by biological fermentation from renewable carbohydrate feedstocks. Prior to the ball milling process, the material was purified by dissolution in chloroform and subsequent precipitation by drop-wise addition to an excess of methanol. The material, in this way, was transformed from pellet to powder form which was necessary for the ball milling process.

Functionalized graphene sheets (FGS) were synthesized by thermal reduction of graphite oxide as described in the first part of this work[23]. Full description of the synthesis and characterization of the FGS can be found elsewhere[24].

2.2 Sample preparation (High energy ball milling - HEBM)

Films of PHBV and PHBV-FGS nanocomposites were prepared. FGS and PHBV powder were milled in the solid state in a Retsch (Germany) centrifugal ball mill (model PM100) and subsequently hot pressed in a hot press (Carver Inc.), just as explained in the previous part of this work[23].

2.3 Characterization

2.3.1 X-ray diffraction (XRD)

X-ray diffraction measurements (XRD) were performed with a Brucker diffractometer (equipped with a continuous scan attachment and a proportional counter) with Ni-filtered Cu Kα radiation (λ= 1.54050 Å). The samples were examined over the angular range of 2º to 40º.

2.3.2 Mass transport properties

Water barrier properties (sorption, diffusion) were evaluated using a microbalance SMS DVS Advantage-2 system. This system has a sensitivity of ±1.0µg, and allows the measurements of mass changes due to sorption or desorption of vapour molecules. In this work the chosen method consisted in submitting the sample to pressure steps at constant temperature. The tests were conducted using water vapour in a nitrogen atmosphere at 30°C. The starting samples were dry, square films having a thickness of 200µm and a side of 15mm. The experimental protocol considered steps of relative humidity from 0 to 98%.

2.3.3 Oxygen transmission rate

The oxygen permeability coefficient was derived from oxygen transmission rate (OTR) measurements recorded using an Oxtran 100 equipment (Modern Control Inc., Minneapolis, MN, US). Experiments were carried out at 24ºC and at 80% relative humidity (RH) conditions. RH was generated by a built-in gas bubbler and was checked

with a hygrometer placed at the exit of the detector. The samples were purged with nitrogen for a minimum of 20 h in the humidity equilibrated samples, prior to exposure to an oxygen flow of 10 ml min^{-1}. A 5 cm^2 sample area was measured by using an in-house developed mask. The measurements were done in duplicate.

2.3.4 Dynamic mechanical analysis (DMA)

Mechanical properties were evaluated using a DMA TAQ800. Measurements were conducted at the constant frequency (1Hz) and amplitude (5µm). The temperature was varied between -30°C and 140°C at 3°C min^{-1}.

2.3.5 Electrical properties

The electrical conductivity was measured at room temperature with a Keithley 6517A electrometer unit in a two-probe resistance measurement configuration controlled by a computer. The source delay for each point of measurement was about 3 s. For each measurement, the sample was placed between two copper electrodes. To enhance the electrical contact between the samples and the electrodes, metallization with Au was used. The metallization was conducted using an Agar Auto Sputter Coater (Agar Scientific Limited-UK-). The metallization time was 180 sec, for a metal deposition of about 22 nm. The electrical conductivity was measured in the voltage range -10 to 10 V. The electrical conductivity, σ (S cm^{-1}), of all the samples was obtained by using the basic Equation (1):

$$\sigma = \frac{L}{\tau W}\frac{1}{R} = \frac{L}{\tau W}\frac{I_{measured}}{V_{applied}} \quad (1)$$

where $R(\Omega)=V_{applied}/I_{measured}$, τ (m), W (m), and L (m) are the resistance, the thickness, the width and the length of the specimens, respectively.

2.3.6. Biodisintegration in composting conditions

The biodesintegration of the samples under controlled composting condition was evaluated according to standard ISO 20200[25]. The solid waste was prepared by mixing 10% of compost (inoculum), 30% rabbit food, 10% starch, 5% sugar, 1% urea, 10% corn oil and 40% sawdust. The inoculum used in the present study was mature compost supplied by Burés Profesional, SA (Girona, España). Prior to the mixing step, the compost was sieved through a 5 mm sieve. According to the standard, the water content was adjusted to 55wt% and kept at this level throughout the whole duration of the experiment by adding water periodically. The samples were cut into squares of 1.5x1.5 cm^2, buried inside the waste at a depth of approximately 6cm and incubated at 58ºC during 90 days inside polypropylene boxes. The specimens were individually sandwiched in between two stainless steel meshes, thus allowing full direct contact with the waste, while simplifying the extraction and labeling of the samples. In order to ensure aerobic conditions to take place, holes were performed on the boxes and, according to the standard, the waste was periodically stirred gently.

The samples were extracted at different disintegration times (7, 15, 27, 41, 56, 69, 76, 83 and 90 days) washed with distilled water, dried at 40ºC under vacuum for 24 h, and weighed. The disintegration degree was determined by normalizing the sample weight for every incubation time to its initial weight.

3. Results and discussion

3.1 Crystal morphology of the nanocomposites

In the previous part of this study[23], DSC analysis under isothermal and non-isothermal conditions showed an influence of FGS incorporation on the kinetics and dynamics of PHBV crystallization. Specifically, the crystallization rate and the homogeneity of the crystals were altered and these effects were strongly dependent on the amount of FGS added to the polymer matrix. It was observed that addition of high concentrations of FGS somehow hindered the crystallization process, i.e. the increase in crystallinity was not as pronounced as with lower FGS contents but, at the same time, more nucleation sites were available, hence increasing the crystallization rate. As a consequence, more heterogeneous crystals and a faster crystallization process were obtained when high FGS concentrations were used.

The crystal structure of the nanocomposite films was studied by X-ray analysis. It has been reported that PHBV exhibits an isodimorphism phenomenon, and it could crystallize in either PHB unit cell or PHV unit cell, depending on the HV content. The transformation from the PHB lattice to the PHV lattice has been reported to occur at about 30 mol % HV[26]. However, Scandola et al.[27] reported that for 34 mol% of HV, PHB crystalline phase was developed, for 55 mol% of HV the X-ray diffraction spectra showed the pattern of the PHV crystalline phase and, interestingly, for 41 mol% of HV, PHB and PHV type crystals coexisted. It has also been previously reported that the reflection at $2\theta = 17^{\circ}$ is associated with the (110) diffraction of PHB lattice, while that at $2\theta = 18^{\circ}$ is associated with the (020) diffraction of PHV lattice[28]. Figure 1 shows the diffractograms of the different samples. The diffractogram of PHBV shows that this

biopolyester is a semicrystalline material with the characteristics reflections from an orthorhombic cell[2, 26, 29]. It can be observed that there was no diffraction peak at 2θ = 18º and, thus, only the typical PHB lattice was developed in the different materials. This result suggests that addition of graphene did not modify the crystalline unit cell since the reflections for the nanocomposites appeared at the same diffraction angles than those from the neat polymer. In fact, the same spacings between planes were obtained for PHBV and its nanocomposites when applying Bragg´s law (cf. **Table 1**) suggesting that the parameters of PHB unit cell were not influenced by FGS addition. Nevertheless the addition of FGS resulted in sharper peaks for the (020) and (110) PHBV reflections if compared to that of pure PHBV. It was related with an increase of the crystallites lamella size, thus confirming that addition of these nanofillers promoted crystallization[29]. Scherrer equation (Equation (2)) was used to determine the crystallite size for the peak corresponding to the (020) reflection of PHBV and its nanocomposites.

$$L(nm) = \frac{K \cdot \lambda}{\beta \cdot \cos\theta} \qquad (2)$$

where K is a dimensionless shape factor with a value close to unity, which is K=0.94 for orthorhombic cell[29], λ is the wavelength of the X-ray radiation which for CuKα radiation is 1.54Å, θ is the Bragg angle and β is the full width half maximum (FWHM). From Table 1 it can be observed that the lamella size for the (020) reflection increased with the addition of FGS, confirming that addition of FGS effectively promoted the crystallization of PHBV, which is in agreement with previous works[29], although the increase observed here was much more pronounced. Moreover, in order to evaluate how the addition of FGS affected the crystal growth, the ratio between the intensity of the peaks related to (020) and (110) crystal planes was calculated and can be seen in Table 1. As observed, an increase in the ratio was noticed with the addition of FGS which

point out that the crystals grew preferentially in the direction of the (020) crystal plane since an increase in the relative intensity of PHBV crystallite in particular direction indicates that the PHBV crystals grow in a preferential orientation along that direction, as previously reported[29].

Therefore, taking into account the DSC analysis performed in a previous work in combination with the X-ray analysis it could be concluded that addition of FGS to the PHBV matrix did not alter the crystalline unit cell, but had an effect on the kinetics and dynamics of PHBV crystallization.

3.2 Mass transport properties

Graphene is considered a promising nanomaterial in gas or liquid-barrier applications because perfect graphene sheets are able to block the diffusion of small molecules. A thorough revision about the use of graphene to improve barrier properties in polymer nanocomposites was carried out by Yoo et al.[7]. However, although a broad range of polymers, graphene types, and processing methods for graphene-based nanocomposite development have been studied, there is no data available for PHBV nanocomposites processed through ball milling. On the contrary, several works have reported about the incorporation of graphene into PHBV matrices[2, 30] but, to the best of our knowledge, the effect of this nanofiller on the transport properties of PHBV have not been previously investigated.

Mass transport properties such as water sorption and diffusion were evaluated for PHBV and PHBV-FGS 3.0 wt% nanocomposite. By measuring the relative increase of weight, undergone with time by samples exposed to the water vapour at a given partial pressure, it is possible to infer the equilibrium concentration of sorbed vapour, C_{eq}

($g_s/100g_p$), where g_s stands for grams of sorbed vapour and g_p stands for grams of polymeric sample. Figure 2a reports the isotherms of water vapour sorption as a function of water activity (a_w), with $a_w = (P/P_0)$, where P and P_0 are the vapour pressure of water and pure water at the same temperature, respectively. Similar water sorption isotherms were reported for PHB, where sorption measurements showed that PHB is a moderately hydrophobic polymer[31]. This hydrophobicity feature was also reported for PHBV by others authors, which is an important advantage not suffering plasticization and swelling[32]. It can be noticed that incorporation of FGS at 3 wt% had no effect in the mechanism of water sorption since no changes in the isotherm were observed when compared with the neat PHBV isotherm.

On the other hand, based on Fickian behaviour, which is a linear dependence of sorption on square root of time t(s), the diffusion coefficient, D ($cm^2\ s^{-1}$), could be calculated from the linear part of the reduced sorption curve according to the Equation (3):

$$\frac{C_t}{C_{eq}} = 4\left(\frac{Dt}{\pi l^2}\right)^{1/2} = \left(\frac{16D}{\pi l^2}\right)^{1/2} t^{1/2} \qquad (3)$$

where C_t and C_{eq} are weight variations at time t and at equilibrium, respectively, l is the sample thickness and D the diffusion coefficient. Furthermore, a well known empirical law is used for polymer-solvent systems which correlate D to C_{eq}, and it is given by the Equation (4):

$$D = D_0 \exp(\gamma\ C_{eq}) \qquad (4)$$

where D_0 is the thermodynamic zero-concentration diffusion coefficient, relative to the condition $C_{eq} = 0$, and γ is the concentration coefficient which depends on the fractional free volume.

Figure 2b shows the diffusion coefficients, D ($cm^2\ s^{-1}$), as function of equilibrium sorbed water, C_{eq} ($g_s/100g_p$). The diffusion behaviour was very similar for both samples

at each concentration. Recently published works, in which cellulose nanowhiskers or keratin were incorporated to PHBV, have reported that only for concentrations of 1 wt% there was a positive effect on water barrier properties. For any other compositions, no effect or even negative effects on water barrier properties were found[22, 33]. In addition, it has also been reported that PHAs have low water vapour permeability, similar to those of conventional thermoplastics, such as low-density polyethylene[34, 35], PVC or PET[36]. Hence, it is thought that due to inherent low water barrier properties of PHBV, fillers, as graphene in this case, find difficulty to improve this property. In fact, water permeability of PHBV copolymer greatly depends on the valerate content. The higher is the valerate content the higher is the water permeability and moisture sensivity, as previously reported[22].

Oxygen permeability measured at 80% RH was evaluated. Figure 3 displays the oxygen permeability of the PHBV and it nanocomposites. A decrease in oxygen permeability was observed for all the nanocomposites in comparison with the neat PHBV. Generally, it could be said that barrier increases with the FGS content, reaching a minimum in permeability value for 3 wt% sample with an improvement of 41%. Previous works have reported a decrease in oxygen permeability using graphene nanoplatelets as fillers[3, 4, 31, 32]. The improved barrier properties was the result of the presence of lamellar structures such as FGS that are homogeneously dispersed in the polymer matrix, as observed in the first part of this work, which can provide a tortuous path inhibiting molecular diffusion through the matrix, consequently, decreasing the gas permeability. The barrier properties are very sensitive to the compatibility at the interface between the matrix and filler phases. An incompatibility at the interface may lead to the generation of micro voids, leading to the higher extents of permeation through the composite materials as a function of filler volume fraction[37]. Thus, these results suggest that good

filler matrix adhesion was obtained since improvements in oxygen barrier properties were obtained, which were mainly related to its planar configuration which created a tortuous path for permeation.

3.3 Dynamic mechanical analysis

In many current applications, polymer and polymer-nanocomposites are subjected to many temperature and frequency fluctuations. In order to evaluate the effect of graphene on temperature dependent relaxation behaviour of PHBV matrix, thermo-mechanical properties were evaluated in some of the samples developed. Figure 4 shows the storage modulus and tan δ, also known as loss factor as a function of temperature as well as the storage modulus at 25ºC and the maximum of tan δ which is related with the glass transition temperature of the nanocomposites. T_g values of the developed materials could not be discerned by a conventional method of T_g measurement by DSC. Nevertheless, the glass transition temperature measured by DMA generally increased with FGS addition. This trend is consistent with previous works where graphene or multi-walled carbon nanotubes (MWNT) were introduced in PHBV[2, 29]. The increase in T_g may be due to the restriction of the chain mobility within the polymer matrix upon FGS addition. The neat PHBV exhibited a tan δ transition around 17ºC, which could be related to the glass transition of the amorphous PHBV molecules[34], whereas for PHBV-FGS nanocomposites the glass transition temperatures were around, 21°C, 19°C, 22°C, and 24ºC for 0.5, 1, 2 and 3 wt% respectively. In fact, at temperatures lower than T_g the loss factor for pristine polymer was higher than for the nanocomposites. This means that higher amounts of energy were dissipated, which could be mainly due to internal frictions of polymer chains which, in turn, were ascribed

to increased mobility of those chains. The results also showed that the FGS nanofiller increased the storage modulus of the neat PHBV in the whole temperature span (cf. Figure 4). However for 0.5 wt% no effects were observed since no changes in the storage modulus curve were noticed. The reinforcing effect of graphene has been previously reported by several authors[2, 11, 19, 20, 35, 36]. Although the storage moduli of nanocomposites were always higher that that for neat polymer, greater increases were observed at low temperatures ("glassy modulus") than those observed at temperatures above Tg ("rubbery modulus"). Evaluation of storage modulus at 25ºC was carried out and, as can be seen, the same trend was noticed, i.e an increase from 2.1 to 2.8 GPa (improvement of 35%) for neat PHBV and PHBV-FGS 3 wt% respectively. The same effects were observed for PHBV-graphene nanocomposites prepared through solution casting[2], and also in PHBV-MWNT prepared by means of direct melt mixing[29]. In addition, previous work incorporating graphene into PLA have reported that storage modulus increased when increasing the graphene content even with small additional amounts of fillers[11]. The homogeneous dispersion of nanofillers and filler-matrix interfacial interactions are important factors in the development of high-performance polymer materials, which are directly related with improvements in mechanical properties. A comparative study of highly and poorly dispersed graphene/epoxy nanocomposites revealed that the highly dispersed graphene fillers are more efficient than the aggregated ones in transferring applied load[38]. In view of the results, it could be thought that good dispersion and filler-matrix adhesion were achieved, being in accordance with the good filler-matrix adhesion suggested in the oxygen barrier properties discussion.

3.4 Electrical properties

A good dispersion of conductive carbonaceous materials such as carbon nanotubes, graphite, graphene and/or its derivatives into polymeric matrices, is widely known to improve the electrical properties of the final materials. Figure 5 shows the electrical conductivities of PHBV and its nanocomposites. Neat PHBV is electrically insulating with a low conductivity (~10^{-13} S cm^{-1}). Nevertheless, the addition of conducting graphene nanofillers significantly increased the conductivity of the materials. The S-shaped curves indicate that the nanocomposites exhibit a typical percolation transition from an insulator to semiconductor[17, 18]. Percolation theory describes the behaviour of connected fillers in a randomly dispersed system. In this case, the connected fillers were functionalized graphene sheets. An analytical model has been previously proposed, based on the Fermi-Dirac distribution, to describe the critical insulator to conductor transition[13].

$$\log(\sigma_c) = \log(\sigma_f) + \frac{\log\left(\frac{\sigma_p}{\sigma_f}\right)}{(1+\exp(t(\phi-\phi_c)))} \quad (5)$$

where σ_c, σ_f and σ_p are the composite, filler, and polymer conductivities, respectively, ϕ is the FGS mass fraction, and t is an empirical parameter that leads to the change in conductivity at the percolation threshold ϕ_c. By assuming a constant value for σ_f and σ_p, from Equation (5) were obtained the best fitted values of ϕ_c and t. Thus, the percolation threshold value of nanocomposites was calculated about ~0.8 wt% (~ 0.3 vol%). It is thought that the low FGS content for electrical percolation threshold is related with the high aspect ratio of FGS and also to a homogeneously and well dispersed nanofiller into the polymer matrix, as observed by SEM and TEM, which allow the conductive filler to form an infinite network of connected paths through the insulating matrix. Room

temperature conductivities (RTC) up to ~0.1 S cm^{-1} were achieved for samples with 3 wt%, sufficient for many electrical applications.

3.5 Biodisintregration in composting conditions

As a biodegradable material, polyhydroxyalkanoates are susceptible to be degraded under natural environmental conditions upon disposal. In order to evaluate the effect of graphene-based fillers addition into PHBV on its biodegradation, biodisintegration of the PHBV and its nanocomposites were studied in composting conditions. Figure 6 shows the biodisintegration (as percentage of weight loss) as a function of time. As observed, despite that some studies about the cyto- and genotoxicity of the grapene have been recently published[39, 40], no remarkable effect upon addition of graphene at different concentrations on the biodegradation process were observed. Nevertheless, it is worth mentioning that an acceleration of the process was mostly observed for the samples loaded with the carbonaceous material since higher weight losses were appreciated at determined tested times for the nanocomposites. Moreover, as observed from Figure 6, the sample with the highest graphene loading was degraded faster. Specifically, while the weight loss of pure PHBV was 33% after 56 days of compost incubation, weight losses of 60% and 94,6% were observed for the samples loaded with 1wt% and 3wt%, respectively. Notwithstanding the faster degradation of the FGS-loaded samples, the overall degradation process of PHBV was not affected, since 90% of disintegration was reached for every studied sample before 75 days.

4. Conclusions

In this paper it was reported the incorporation of functionalized graphene sheets (FGS) within a PHBV matrix through ball milling. The resulted nanocomposites showed improved physical properties. Specifically, X-ray diffraction, in combination with isothermal and non-isothermal crystallization studies performed in the first part of this work, confirmed that addition of FGS did not modify the crystal structure of the PHBV matrix. An increase in the oxygen barrier properties was observed upon addition of FGS mainly related to its planar configuration which created a tortuous path for permeation, also corroborating good filler-matrix interfacial interaction. On the contrary, due to the high hydrophobicity of PHBV matrix, no effects were observed in terms of water vapour mass transport properties. Addition of FGS resulted in an increase in the storage modulus mainly due to the reinforcing effect of FGS homogeneously dispersed in the PHBV matrix. The electrical percolation threshold of PHBV-FGS nanocomposites was attained at ~ 0.3 vol%, increasing the PHBV matrix conductivity 12 log units and reaching a room temperature conductivity of up to ~0.1 S cm^{-1}. Therefore, it could be concluded that this work provides new evidences of a suitable compounding method, i.e. the ball milling technique, to develop graphene-based nanocomposites, with enhanced gas barrier, mechanical and electrical properties.

Acknowledgements

J Ambrosio-Martín would like to thank the Spanish Ministry of Economy and Competitiveness for the FPI grant BES-2010-038203. M.J. Fabra is recipient of a "Juan de la Cierva" contract from the Spanish Ministry of Economy and Competitiveness. The

authors acknowledge financial support from the MINECO (MAT2012-38947-C02-01 project) and from the FP7 ECOBIOCAP project.

References

1. Marques, P. A. A. P.; Gonçalves, G.; Cruz, S.; Almeida, N.; Singh, M. K.; Grácio, J.; Suosa, A. C. M., Functionalized Graphene Nanocomposites, 2011.

2. Sridhar, V.; Lee, I.; Chun, H. H.; Park, H., *Exp. Polym. Lett.* **2013**, 7, 320-328.

3. Jiang, X.; Drzal, L. T., *J. Pow. Sour.* **2012**, 218, 297-306.

4. Pinto, A. M.; Cabral, J.; Tanaka, D. A. P.; Mendes, A. M.; Magalhães, F. D., *Polym. Int.* **2013**, 62, 33-40.

5. Compton, O. C.; Kim, S.; Pierre, C.; Torkelson, J. M.; Nguyen, S. T., *Adv. Mater.* **2010**, 22, 4759-4763.

6. Schniepp, H. C.; Li, J. L.; McAllister, M. J.; Sai, H.; Herrera-Alonson, M.; Adamson, D. H.; Prud'homme, R. K.; Car, R.; Seville, D. A.; Aksay, I. A., *J. Phys. Chem. B* **2006**, 110, 8535-8539.

7. Yoo, B. M.; Shin, H. J.; Yoon, H. W.; Park, H. B., *J. Appl. Polym. Sci.* **2014**, 131,

8. El Achaby, M.; Arrakhiz, F. Z.; Vaudreuil, S.; Essassi, E. M.; Qaiss, A.; Bousmina, M., *J. Appl. Polym. Sci.* **2013**, 127, 4697-4707.

9. Ding, P.; Su, S.; Song, N.; Tang, S.; Liu, Y.; Shi, L., *Carbon* **2014**, 66, 576-584.

10. Fang, M.; Wang, K.; Lu, H.; Yang, Y.; Nutt, S., *J. Mater. Chem.* **2009**, 19, 7098-7105.

11. Bao, C.; Song, L.; Xing, W.; Yuan, B.; Wilkie, C. A.; Huang, J.; Guo, Y.; Hu, Y., *J. Mater. Chem.* **2012**, 22, 6088-6096.

12. Kim, I. H.; Jeong, Y. G., *J. Polym. Sci, Part B: Polym. Phys.* **2010**, 48, 850-858.

13. Gorrasi, G.; Di Lieto, R.; Patimo, G.; De Pasquale, S.; Sorrentino, A., *Polymer* **2011**, 52, 1124-1132.

14. Gorrasi, G.; Sarno, M.; Di Bartolomeo, A.; Sannino, D.; Ciambelli, P.; Vittoria, V., *J. Polym. Sci, Part B: Polym. Phys.* **2007**, 45, 597-606.

15. Vertuccio, L.; Gorrasi, G.; Sorrentino, A.; Vittoria, V., *Carbohydr. Polym.* **2009**, 75, 172-179.

16. Perrin-Sarazin, F.; Sepehr, M.; Bouaricha, S.; Denault, J., *Polym. Eng. Sci.* **2009**, 49, 651-665.

17. Wu, H.; Zhao, W.; Chen, G., *J. Appl. Polym. Sc.* **2012**, 125, 3899-3903.

18. Wu, H.; Zhao, W.; Hu, H.; Chen, G., *J. Mater. Chem.* **2011**, 21, 8626-8632.

19. Wang, J.; Wang, X.; Xu, C.; Zhang, M.; Shang, X., *Polym. Int.* **2011**, 60, 816-822.

20. El Achaby, M.; Qaiss, A., *Mater. Des.* **2013**, 44, 81-89.

21. Stankovich, S.; Dikin, D. A.; Dommett, G. H. B.; Kohlhaas, K. M.; Zimney, E. J.; Stach, E. A.; Piner, R. D.; Nguyen, S. T.; Ruoff, R. S., *Nature* **2006**, 442, 282-286.

22. Martínez-Sanz, M.; Villano, M.; Oliveira, C.; Albuquerque, M. G. E.; Majone, M.; Reis, M.; Lopez-Rubio, A.; Lagaron, J. M., *New Biotechnol.* **2014**, 31, 364-376.

23. Ambrosio-Martín, J.; Gorrasi, G.; Lopez-Rubio, A.; Fabra, M. J.; Cabedo, L.; López-Manchado, M.A.; Lagaron, J. M., *J. Appl. Poly. Sc.* **2014**, unpublished,

24. Verdejo, R.; Barroso-Bujans, F.; Rodriguez-Perez, M. A.; De Saja, J. A.; Lopez-Manchado, M. A., *J. Mater. Chem.* **2008**, 18, 2221-2226.

25. ISO Standard 20200:2004. "Determination of the degree of disintegration of plastic materials under simulated composting conditions in a laboratory-scale test". International Organization for Standardization.

26. Kunioka, M.; Tamaki, A.; Doi, Y., *Macromolecules* **1989**, 22, 694-697.

27. Scandola, M.; Ceccorulli, G.; Pizzoli, M.; Gazzano, M., *Macromolecules* **1992**, 25, 1405-1410.

28. Shan, G. F.; Gong, X.; Chen, W. P.; Chen, L.; Zhu, M. F., *Colloid Polym. Sci.* **2011**, 289, 1005-1014.

29. Vidhate, S.; Innocentini-Mei, L.; D'Souza, N. A., *Polym. Eng. Sci.* **2012**, 52, 1367-1374.

30. Wang, B. J.; Zhang, Y. J.; Zhang, J. Q.; Gou, Q. T.; Wang, Z. B.; Chen, P.; Gu, Q., *Chinese Journal of Polymer Science (English Edition)* **2013**, 31, 670-678.

31. Kalaitzidou, K.; Fukushima, H.; Drzal, L. T., *Carbon* **2007**, 45, 1446-1452.

32. Potts, J. R.; Dreyer, D. R.; Bielawski, C. W.; Ruoff, R. S., *Polymer* **2011**, 52, 5-25.

33. Pardo-Ibáñez, P.; Lopez-Rubio, A.; Martínez-Sanz, M.; Cabedo, L.; Lagaron, J. M., *J. Appl. Polym. Sci.* **2014**, 131,

34. Cimmino, S.; Iodice, P.; Silvestre, C.; Karasz, F. E., *J. Appl. Polym. Sci.* **2000**, 75, 746-753.

35. Zhao, J.; Wang, X.; Zhou, W.; Zhi, E.; Zhang, W.; Ji, J., *J. Appl. Polym. Sci.* **2013**, 130, 3212-3220.

36. Zhao, X.; Zhang, Q.; Chen, D.; Lu, P., *Macromolecules* **2010**, 43, 2357-2363.

37. Sorrentino, A.; Gorrasi, G.; Vittoria, V. In Environmental Silicate Nano-Biocomposites; Avérous, L.; Pollet, E., Eds.; Springer London, **2012**, Chap. 9, pp 237-264

38. Tang, L. C.; Wan, Y. J.; Yan, D.; Pei, Y. B.; Zhao, L.; Li, Y. B.; Wu, L. B.; Jiang, J. X.; Lai, G. Q., *Carbon* **2013**, 60, 16-27.

39. Akhavan, O.; Ghaderi, E.; Akhavan, A., *Biomaterials* **2012**, 33, 8017-8025.

40. Akhavan, O.; Ghaderi, E.; Emamy, H.; Akhavan, F., *Carbon* **2013**, 54, 419-431.

Figures

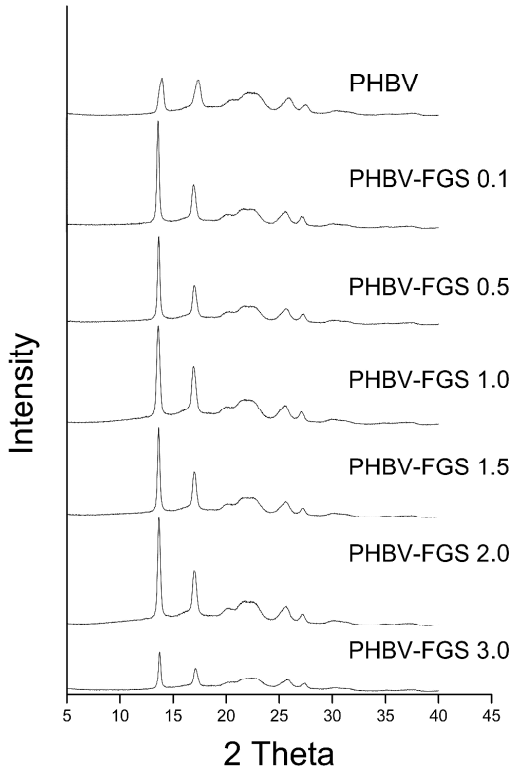

Figure 1. X-ray patterns of PHBV and its nanocomposites

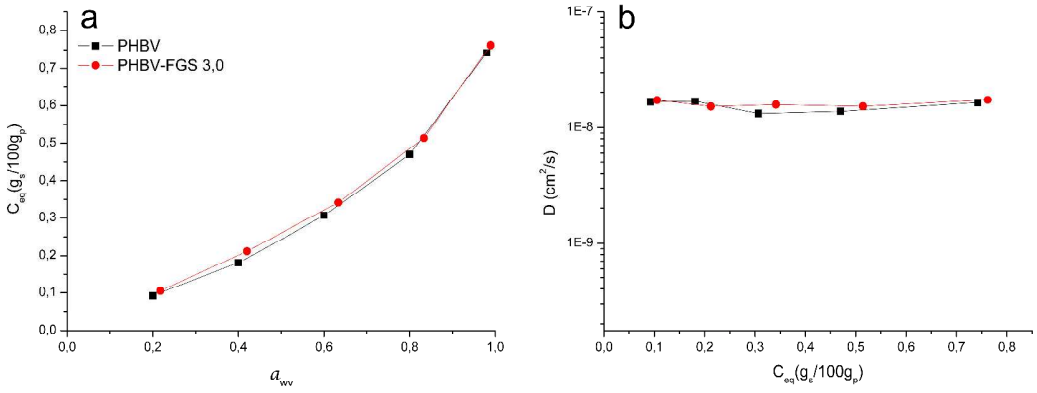

Figure 2. Sorption isotherms as function of water vapour activity (a_w) (a) and diffusion coefficients versus equilibrium sorbed water (C_{eq}) (b) of water vapour for pure PHBV and PHBV-FGS 3.0 wt% nanocomposites.

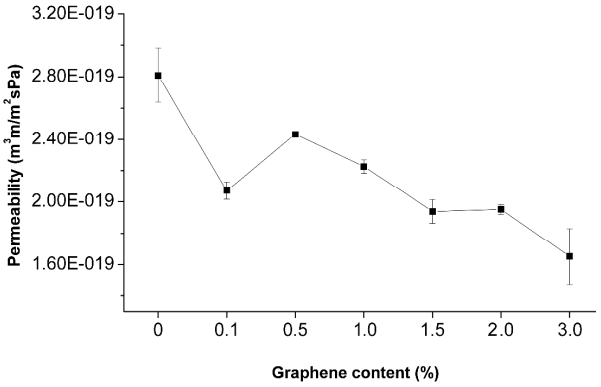

Figure 3. Oxygen permeability of pure PHBV and its nanocomposites with FGS.

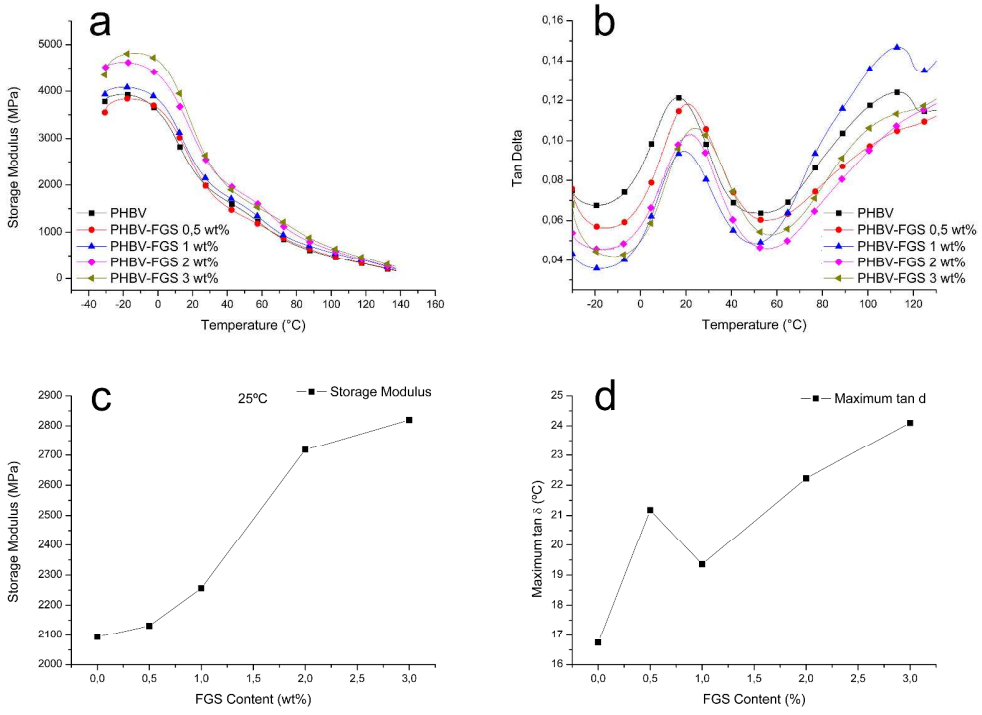

Figure 4. Dynamo-mechanical analysis of PHBV and its nanocomposites. Storage modulus (a) and tan δ (b) versus temperature curves, storage modulus at 25ºC (c) and maximum of tan δ (d).

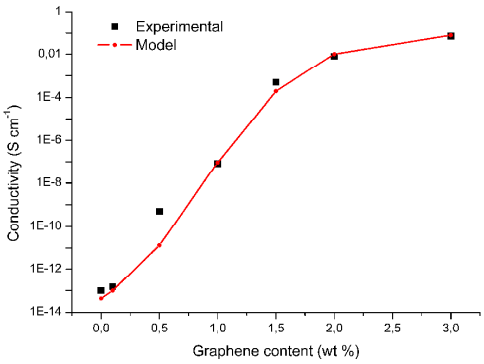

Figure 5. Experimental and calculated electrical conductivity versus filler loading for PHBV-FGS nanocomposites.

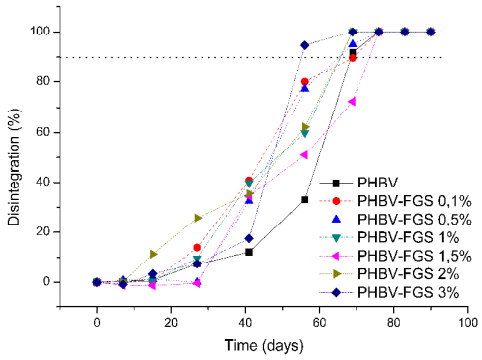

Figure 6. Loss in weight as a result of the biodegradation of PHBV and PHBV-FGS nanocomposites in composting conditions for up to 90 days.

Table 1. Calculated lamellar spacing and crystallite sizes of PHBV and its nanocomposites with FGS.

	d-spacing (nm)	Crystal size L_{020} (nm)	$I_{(020)}/I_{(110)}$
PHBV	0.64	16.29	1.1
PHBV-FGS 0,1 %	0.65	30.80	2.3
PHBV-FGS 0,5 %	0.65	30.45	2.1
PHBV-FGS 1 %	0.65	29.88	1.6
PHBV-FGS 1,5 %	0.65	30.07	1.9
PHBV-FGS 2 %	0.65	26.49	1.9
PHBV-FGS 3 %	0.65	27.44	1.6

Figure Captions

Figure 1. X-ray patterns of PHBV and its nanocomposites

Figure 2. Sorption isotherms as function of water vapour activity (a_w) (a) and diffusion coefficients versus equilibrium sorbed water (C_{eq}) (b) of water vapour for pure PHBV and PHBV-FGS 3.0 wt% nanocomposites.

Figure 3. Oxygen permeability of pure PHBV and its nanocomposites with FGS.

Figure 4. Dynamo-mechanical analysis of PHBV and its nanocomposites. Storage modulus (a) and tan δ (b) versus temperature curves, storage modulus at 25ºC (c) and maximum of tan δ (d).

Figure 5. Experimental and calculated electrical conductivity versus filler loading for PHBV-FGS nanocomposites.

Figure 6. Loss in weight as a result of the biodegradation of PHBV and PHBV-FGS nanocomposites in composting conditions for up to 90 days.

Tables

Table 1. Calculated lamellar spacing and crystallite sizes of PHBV and its nanocomposites with FGS.

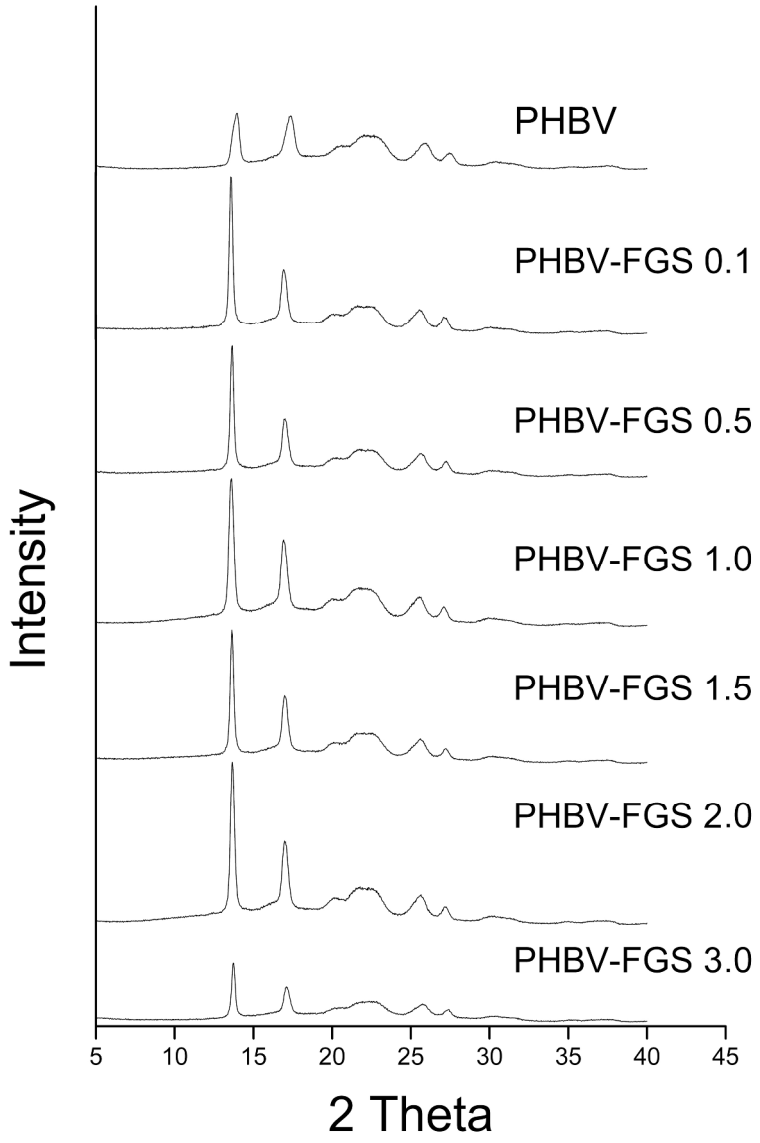

Figure 1. X-ray patterns of PHBV and its nanocomposites
120x172mm (600 x 600 DPI)

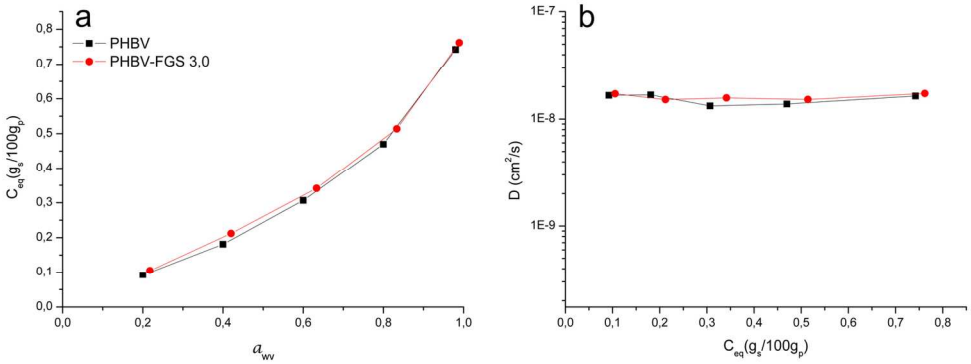

Figure 2. Sorption isotherms as function of water vapour activity (aw) (a) and diffusion coefficients versus equilibrium sorbed water (Ceq) (b) of water vapour for pure PHBV and PHBV-FGS 3.0 wt% nanocomposites.
71x29mm (600 x 600 DPI)

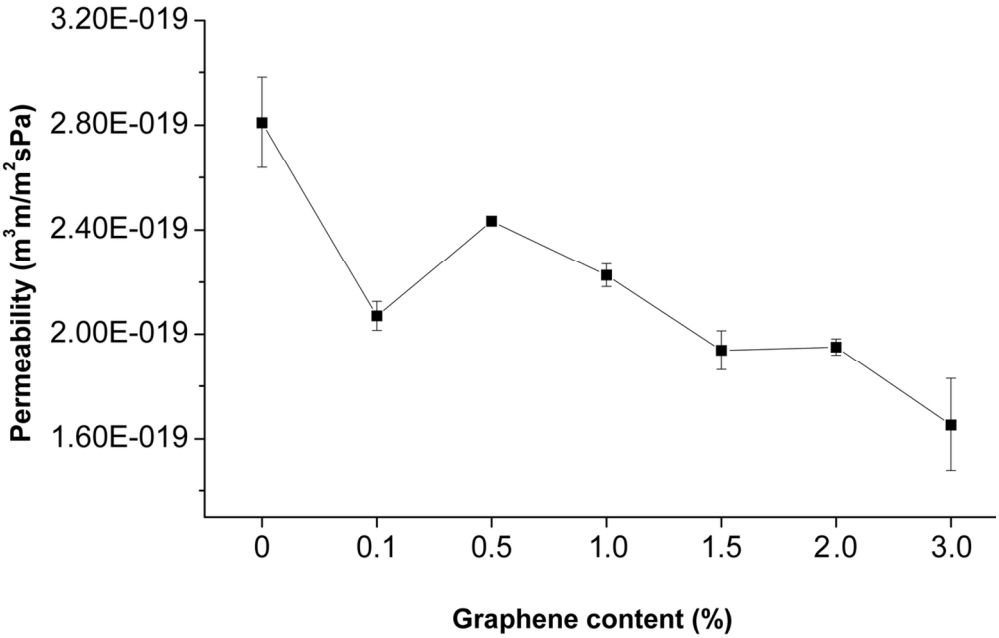

Figure 3. Oxygen permeability of pure PHBV and its nanocomposites with FGS.
59x41mm (600 x 600 DPI)

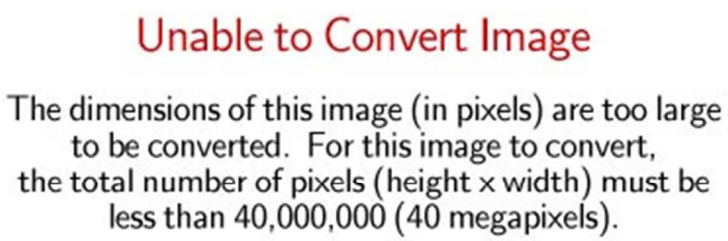

Figure 4. Dynamo-mechanical analysis of PHBV and its nanocomposites. Storage modulus (a) and tan δ (b) versus temperature curves, storage modulus at 25ºC (c) and maximum of tan δ (d).

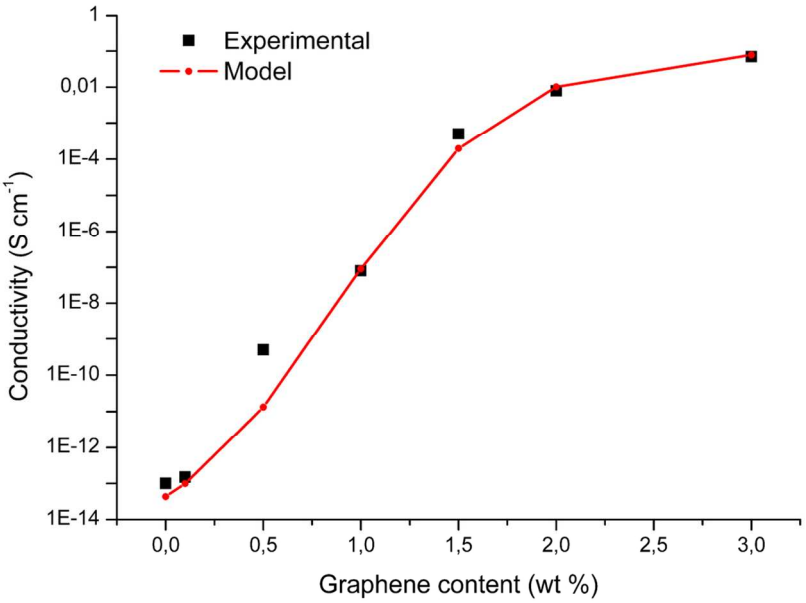

Figure 5. Experimental and calculated electrical conductivity versus filler loading for PHBV-FGS nanocomposites.
58x41mm (600 x 600 DPI)

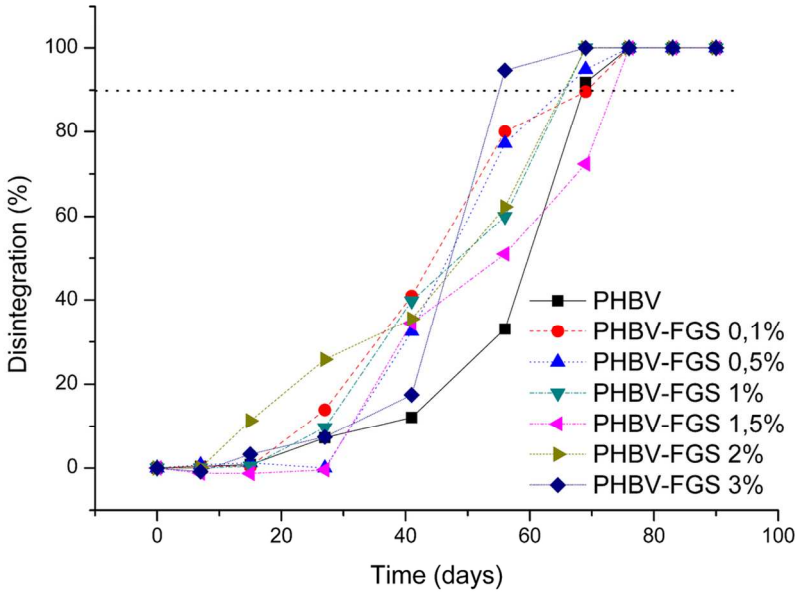

Figure 6. Loss in weight as a result of the biodegradation of PHBV and PHBV-FGS nanocomposites in composting conditions for up to 90 days.
58x41mm (600 x 600 DPI)

Table 1. Calculated lamellar spacing and crystallite sizes of PHBV and its nanocomposites with FGS.

	d-spacing (nm)	Crystallite size L_{020} (nm)	$I_{(020)}/I_{(110)}$
PHBV	0.64	16.29	1.1
PHBV-FGS 0,1 %	0.65	30.80	2.3
PHBV-FGS 0,5 %	0.65	30.45	2.1
PHBV-FGS 1 %	0.65	29.88	1.6
PHBV-FGS 1,5 %	0.65	30.07	1.9
PHBV-FGS 2 %	0.65	26.49	1.9
PHBV-FGS 3 %	0.65	27.44	1.6